Understanding COVID-19 epidemics: a multi-scale modeling approach

Maíra Aguiar, Vizda Anam, Nicole Cusimano, Damián Knopoff and Nico Stollenwerk

Abstract COVID-19 was declared a pandemic by the World Health Organization in March 2020 and, since then, research on mathematical modeling became imperative and very influential to understand the epidemiological dynamics of disease spreading and control under different scenarios. In this chapter, two different approaches to model the spread of COVID-19 are presented. The model frameworks are described and results are presented in connection with the current epidemiological situation of vaccination roll-out. This chapter is structured as follows. Section 2 presents the stochastic SHARUCD modeling framework developed withing a modeling task force created to support public health managers during the COVID-19 crisis. As an extension of the basic SHAR (Susceptible-Hospitalized-Asymptomatic-Recovered) model, the SHARUCD models were parameterized and validated with empirical data for the Basque Country, Spain, and have been used (up until now) to monitor COVID-19 spreading and control over the course of the pandemic. Section 3 introduces the kinetic theory of active particles (KTAP) model for the spread of a disease. With an exploratory analysis, we present a possible way to deal with heterogeneity and

Maíra Aguiar

Basque Center for Applied Mathematics, Mazarredo 14, Bilbao, Spain e-mail: maguiar@bcamath.org

Vizda Anam

Basque Center for Applied Mathematics, Mazarredo 14, Bilbao, Spain e-mail: vanam@bcamath.org

Nicole Cusimano

Basque Center for Applied Mathematics, Mazarredo 14, Bilbao, Spain e-mail: ncusimano@bcamath.org

Damián Knopoff

Basque Center for Applied Mathematics, Mazarredo 14, Bilbao, Spain e-mail: dknopoff@bcamath.org

Nico Stollenwerk

Basque Center for Applied Mathematics, Mazarredo 14, Bilbao, Spain e-mail: nico.biomath@gmail.com

multiscale features. Section 4 concludes this work, with a discussion on both models and further research perspectives description.

1 Introduction

More than eighteen months have passed since a severe respiratory syndrome (COVID-19) caused by a new coronavirus (SARS-CoV-2) was identified in China [58], and spread rapidly around the globe. COVID-19 was declared a pandemic by the World Health Organization (WHO) in March, 2020 [59, 24]. As of the beginning of August, 2021, around 200 million cases were confirmed with more than 4 million deaths, a global case fatality ratio of approximately 2% [57, 60].

COVID-19 symptoms can range from asymptomatic/mild to severe illness, and disease severity and death occurring according to a hierarchy of risks [9], with age and pre-existing health conditions enhancing disease severity. With an unprecedented global health burden arising, the collective behavior of societies has been significantly affected by the extreme measures implemented to control disease transmission. Leading to serious social economic problems, the COVID-19 pandemic is considered by the World Bank Global Economic Prospects to have caused the deepest global recession since the second World War (WW II) [61].

Vaccines against COVID-19 have been developed in record time and are now globally distributed. With different efficacies, COVID-19 vaccines are remarkably effective against severe disease. However, the so-called sterilizing immunity, occurring when vaccinated individuals cannot transmit the virus, is still being evaluated. Four vaccines are now licensed for emergency use in Europe: two mRNA-type vaccines, Pfizer-BioNTech and Moderna, with about 95% vaccine efficacy after second dose, and two viral vector vaccines, the ones by Oxford-AstraZeneca and Johnson & Johnson's Janssen, with about 70% vaccine efficacy upon full immunization, i.e., with two doses in the first case and one dose in the latter [14, 25, 28, 41, 45, 55]. Note that the above-mentioned vaccine efficacies are under constant evaluation, especially now that new SARS-CoV-2 variants have been identified.

In Spain, the new coronavirus infection was first notified on January 1st, 2020, and by March 13, cases had been confirmed in all 50 provinces of the country. A nationwide State of Alarm was declared on March 15, 2020 with a national lockdown becoming effective on March 16, 2020. All residents were mandated to remain in their normal residences except to purchase food and medicines, work or attend emergencies. Lockdown restrictions also mandated the temporary closure of non-essential shops and businesses, including bars, restaurants, cafes, cinemas, commercial and retail businesses. In the Basque Country, an autonomous community in northern Spain with 2.2 million inhabitants, the first cases of COVID-19 were notified on March 4, 2020. Ruled by the same Spanish decrees, lockdown measures were implemented accordingly and in time.

Research on mathematical modeling became imperative and very influential to understand the epidemiological dynamics of COVID-19 spreading and control over

the course of the pandemic under different scenarios. An enormous quantity of epidemiological modeling peer reviewed articles and preprints studying COVID-19 dynamics have appeared since the pandemic started. Aiming to predict the spread of the disease in a population, modeling task forces were created around the globe. Using, most of the time, simple models such as the SIR (Susceptible-Infected-Recovered) or SEIR (Susceptible-Exposed-Infected-Recovered) in mechanistic or probabilistic frameworks, researchers were requested to provide projections about specific disease-related variables such as hospitalizations, intensive care units admissions (ICUs) and deaths.

Already in March 2020, a multidisciplinary task force (the Basque Modeling Task Force, BMTF) was created to assist the Basque health managers and Government during the COVID-19 responses. Within the BMTF, a stochastic SHARUCD modeling framework was developed [1, 2, 5, 10, 47]. As an extension of the simple SIR model, this flexible framework considers populations of susceptible individuals (S), severe cases prone to hospitalization (H), mild, sub-clinical or asymptomatic (A), recovered (R), and patients admitted to intensive care units (U). The recorded cumulative positive cases, which includes all new positive cases for each class of H, A, U, R, are counted within the C classes, including the deceased (D) cases.

Able to describe the COVID-19 epidemic in terms of disease spreading, the SHARUCD model gives accurate projections (see Fig. 1) on hospitalizations, ICU admissions, and deceased cases from March 2020 to December 2020, when vaccination roll-out started. The modeling framework was used to monitor the COVID-19 epidemiological dynamics in the Basque Country while the lockdown measures were relaxed and tightened over time, evaluating also the impact of non-pharmaceutical interventions and social distancing.

It is worth stressing that in order to build useful models a close collaboration with field epidemiologists, laboratory researchers in virology, immunology, and biology, as well as with public health stakeholders is needed [3, 8, 11, 12]. Moreover, a constant good data input is essential for model parameterization and validation [6, 7, 34, 43].

Modeling refinements were validated by epidemiological data continuously collected and provided by the Basque Health Department and the Basque Health Service (Osakidetza). Results on the evolution of the epidemic in the Basque Country are regularly updated and publicly available on the "SHARUCD Dashboard" [53].

The SHARUCD modeling framework and its refinements will be presented in the first part of this chapter. Basic concepts on vaccination towards herd immunity and the impact of vaccination roll-out, considering heterogeneity on vaccine efficacy for hospitalization and overall infection, will also be discussed.

Population heterogeneity is also an important feature to be considered when evaluating the effects of control measures applied to different segments of society. For example, pre-existing comorbidities and age are considered important factors affecting disease severity during the COVID-19 pandemic [9, 32] and, for that, the use of an age-structured population modeling approach would be appropriate to quantify the role of different age groups on disease spreading and to evaluate the impact of intervention measures for each population stratum (e.g., [4, 26, 27]).
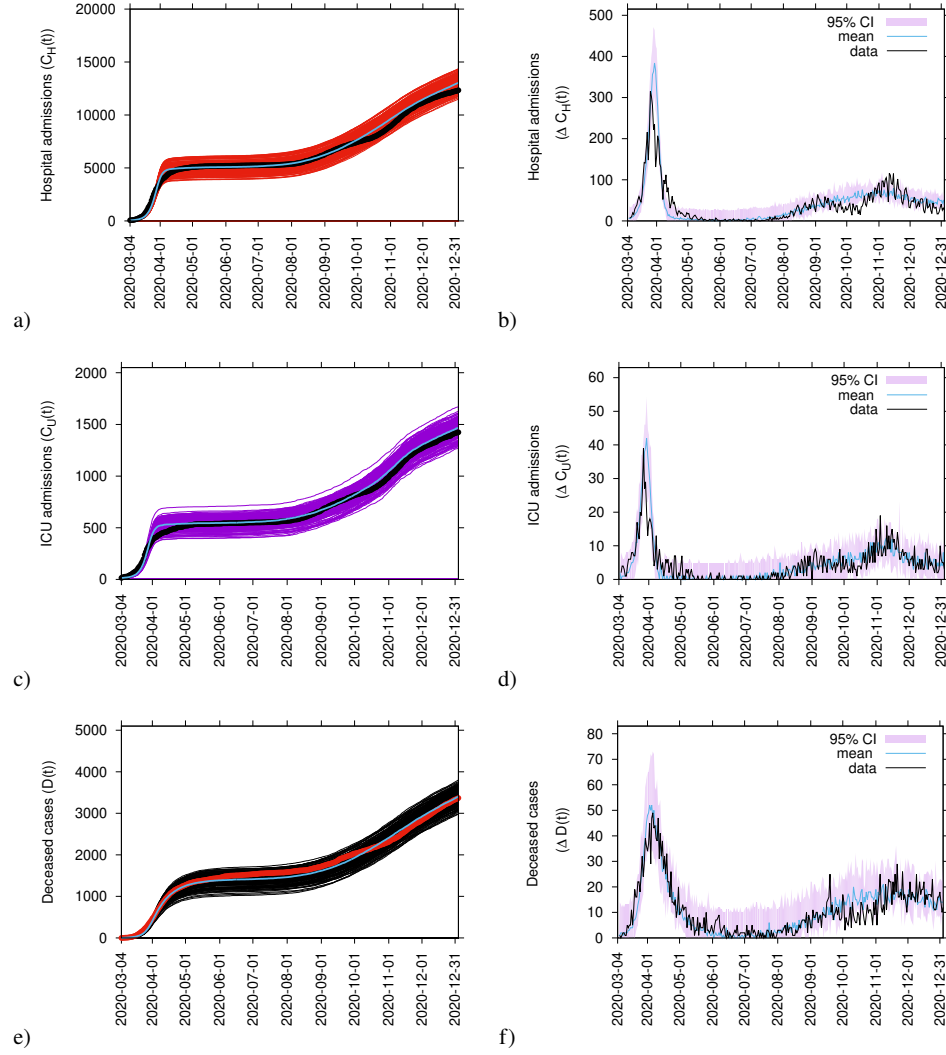
Fig. 1 From March 4 to December 31, 2020, on the left hand side we plot the ensemble of stochastic realizations of the SHARUCD-model for cumulative cases. In a) cumulative hospitalized cases $C_H(t)$, in c) cumulative ICU admissions $C_U(t)$ and in e) cumulative deceases cases $D(t)$. The mean of the stochastic realizations is plotted in light blue. Empirical data is plotted as black dots for hospitalizations and ICU admissions, and red dots for deceased cases. On the right hand side we plot the model results for the daily incidences. In b) daily hospitalized cases, in d) daily ICU admissions and in f) daily deceased cases. Empirical data are plotted as a black line for all three cases while the mean of 200 stochastic realizations is plotted in light blue. The 95% confidence intervals are obtained empirically from the stochastic realizations and are plotted as light purple shadow.

Some useful contributions in this direction are provided by [37, 44], for example, where age-structured models for SARS-CoV-2 fitted to hospital admission and seroprevalence data were used to estimate the impact of school contacts on transmission of the disease and to assess the effects of school-based measures, modeling interactions using mixing matrices [42].

There are, however, many different ways to include heterogeneity in dynamical models. In this chapter, we will also present an exploratory exercise using a modeling approach based on the kinetic theory of active particles (KTAP) published in [17]. The KTAP approach is very versatile since it allows the population to be subdivided into functional subsystems (FS) according to the problem under study. For instance, age structure or population with comorbidities can be easily introduced to stratify the population with a social network structure [4].

The KTAP approach also deals with the multiscale nature of the system under study. Besides discussion on contagion at the level of a population, where the virus is transmitted from infected to healthy individuals by short-range interactions, the complexity of the system increases with the inclusion of multiscale information, such as within-host features [23]. In this case, the micro-scale corresponds to virus particles and immune cells, which induce the dynamics at the higher scale of individuals who carry an infection, at meso-scale level, also affecting the collective behavior of individuals which are then analyzed at the macro-scale level [17], see illustration in Fig. 2.
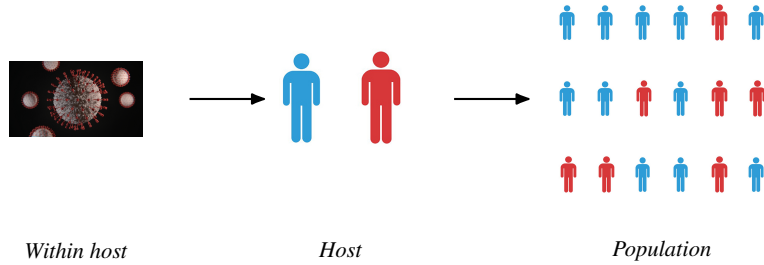

Within host   *Host*   *Population*

Fig. 2 Schematic representation of different scale dynamics. COVID-19 virus image on the left credit: Photo by Viktor Forgacs on Unsplash.

This chapter is structured as follows. Section 2 presents the SHARUCD model and its refinements, both in the stochastic and deterministic versions, which are being successfully used to assist public health managers and policy makers in the Basque Country, Spain. Section 3 introduces the KTAP model for the spread of a disease. With an exploratory analysis, a possible way to deal with heterogeneity and multiscale features is presented. Section 4 concludes this work, with a discussion on both models, presenting the connection of this research with the current epidemiological situation of vaccine impact and further research perspectives.

2 Mathematical modeling applied to infectious diseases: COVID-19 as a case study

Epidemiological models are formal frameworks to convey ideas about the components of a host-pathogen interaction and can be used as a tool to understand and predict the spread of infectious diseases as well as to evaluate the impact of control measures in different epidemiological scenarios.

Mathematical models were introduced into infectious disease epidemiology in the early 20th century, and a series of deterministic compartmental models such as SIS (susceptible-infected-susceptible) and SIR (susceptible-infected-recovered) have been proposed based on the flow patterns between compartments of hosts in a population, which is divided into different subgroups for the considered disease-related stages.

One way to visualize these models is by using state-flow diagrams, see Fig. 3, where circles represent the compartments for each disease-related stage and arrows indicate the transitions for disease progression.

Disease propagation is an inherently stochastic phenomenon and there are a number of reasons why one should use stochastic models to capture the disease transmission process. However, the mean-field approximation, where the dynamics of the mean quantities are approximated by neglecting correlations, is often used as a good approximation to get a first understanding of the behavior of stochastic systems in certain parameter regions [40, 50, 52].

2.1 The SIR and SHAR models

The SIR (susceptible-infected-recovered) model, see Fig. 3 b), is one of the simplest compartmental models, dividing the observed population into three groups: the class S of susceptible individuals to the considered disease, the class of infected individuals I, and the class R of individuals who have recovered from the infection. In analogy with chemical reactions, the dynamics within the typical SIR framework with infection rate β, recovery rate γ and waning immunity rate α can be illustrated by the scheme

$$
\begin{aligned}
S + I &\xrightarrow{\beta} I + I \\
I &\xrightarrow{\gamma} R \\
R &\xrightarrow{\alpha} S
\end{aligned}
\tag{1}
$$

which translates into the following ODE system describing the temporal evolution of the number of individuals in each of the three model compartments:
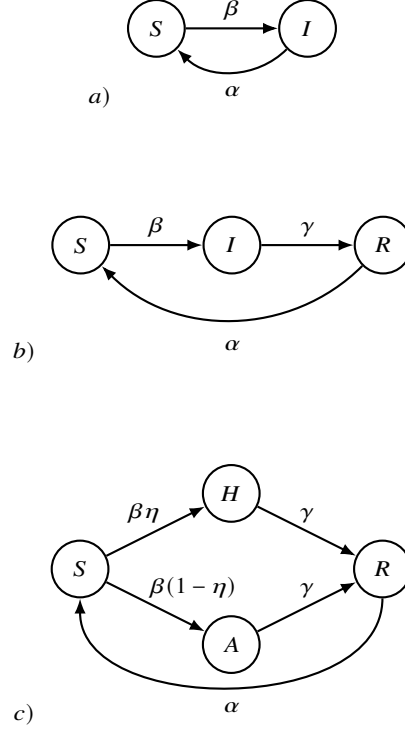
Fig. 3 State-flow diagram of simple epidemiological models. disease-related stages are susceptibles S, Infected I, and eventually stratified as asymptomatic A or hospitalized H, and recovered R. In a) the SIS type model, in b) the SIR type model, and in c) the SHAR type model. For a host population of N individuals, with infection rate β, recovery rate γ and waning immunity rate α. In the SHAR type model, η is the proportion of infected individuals prone to hospitalization, while $1 - \eta$ will develop mild/asymptomatic infection.

$$\frac{dS}{dt} = \alpha R - \beta \frac{S}{N} I,$$

$$\frac{dI}{dt} = \beta \frac{S}{N} I - \gamma I, \tag{2}$$

$$\frac{dR}{dt} = \gamma I - \alpha R,$$

with N denoting the population size, i.e., $N = S + I + R$.

The stochastic SIR epidemic is modeled as a time-continuous Markov process to capture population noise. The temporal dynamics for the probability $p(S, I, t)$ of having an integer number S of susceptible and I of infected individuals at time t can be given as the following master equation [54]

$$\frac{d}{dt}p(S, I, t) = \frac{\beta}{N}(S+1)(I-1)\ p(S+1, I-1, t)$$
$$+\gamma(I+1)p(S, I+1, t)$$
$$+\alpha(N-(S-1)-I)\ p(S-1, I, t) \tag{3}$$
$$-\left(\frac{\beta}{N}SI + \gamma I + \alpha(N-S-I)\right)\ p(S, I, t),$$

while the number of recovered individuals follows from the constant population size assumption $R = N - (S + I)$. Letting $\mathbf{x}$ denote the state vector of densities, the master equation for the probabilities $p(\mathbf{x}, t)$ can be expressed in terms of n transitions $w_j(\mathbf{x})$ and small deviations from state $\mathbf{x}$ given by $\Delta \mathbf{x}_j$ as

$$\frac{d}{dt}p(\mathbf{x}, t) = \sum_{j=1}^{n}\left(Nw_j(\mathbf{x}+\Delta\mathbf{x})p(\mathbf{x}+\Delta\mathbf{x}_j, t) - Nw_j(\mathbf{x})p(\mathbf{x}, t)\right), \tag{4}$$
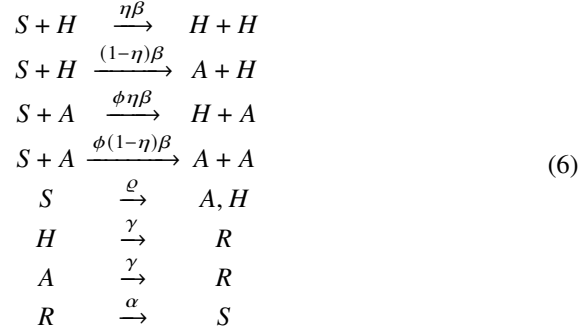
where $\Delta\mathbf{x}_j := \frac{1}{N}\mathbf{r}_j$ for suitable shifting vectors $\mathbf{r}_j$. Specifically, for the SIR model described above, we have $\mathbf{x} := (x_1, x_2)^T$ with $x_1 := S/N$ and $x_2 := I/N$, $n = 3$, and the following transitions $w_j(\mathbf{x})$ with corresponding shifting vectors $\mathbf{r}_j$:

$$\begin{array}{ll}
w_1(\mathbf{x}) = \beta x_1 x_2 & , \mathbf{r}_1 = (1, -1)^T \\
w_2(\mathbf{x}) = \gamma x_2 & , \mathbf{r}_2 = (0, 1)^T \\
w_3(\mathbf{x}) = \alpha(1 - x_1 - x_2) & , \mathbf{r}_3 = (-1, 0)^T
\end{array} \tag{5}$$

This process can be simulated by the Gillespie algorithm giving stochastic realizations of infected and susceptible individuals in time [30, 31].

To distinguish between mild and severely infected cases, the SIR framework can be extended into the so-called SHAR model, see Fig. 3 c), where H stands for individuals developing a severe form of the disease and likely being hospitalized, while A refers to infected individuals who are asymptomatic or have a mild form of the disease. This system includes two additional epidemiological parameters: η and ϕ. While the severity ratio η gives the fraction of infected individuals who develop severe symptoms (and hence $1 - \eta$ gives the asymptomatic fraction of infections), the parameter ϕ is a scaling factor used to differentiate the infectivity $\phi\beta$ of mild/asymptomatic infections with respect to the baseline infectivity β of severe/hospitalized cases. The value of ϕ can be tuned to reflect different situations: a value of $\phi < 1$ reflects the fact that severe cases have larger infectivity than mild cases (e.g., due to enhanced coughing and sneezing), while $\phi > 1$ indicates that asymptomatic individuals and mild cases contribute more to the spread of the infection (e.g., due to their higher mobility and possibility of interaction) than the severe cases which are more likely to be detected and isolated [10].

In the case of COVID-19, we assume $\phi > 1$, since severe cases are likely hospitalized and isolated while mild/asymptomatic cases are often undetected and hence able to transmit the disease, contributing significantly more to the force of infection than the severe cases. The model dynamics can be illustrated by the following reaction scheme

$$
\begin{aligned}
S + H &\xrightarrow{\eta\beta} H + H \\
S + H &\xrightarrow{(1-\eta)\beta} A + H \\
S + A &\xrightarrow{\phi\eta\beta} H + A \\
S + A &\xrightarrow{\phi(1-\eta)\beta} A + A \\
S &\xrightarrow{\varrho} A, H \\
H &\xrightarrow{\gamma} R \\
A &\xrightarrow{\gamma} R \\
R &\xrightarrow{\alpha} S
\end{aligned}
\tag{6}
$$

and the corresponding SHAR ODE system

$$
\begin{aligned}
\frac{dS}{dt} &= \alpha R - \beta\frac{S}{N}(H + \phi A + \varrho N), \\[2mm]
\frac{dH}{dt} &= \eta\beta\frac{S}{N}(H + \phi A + \varrho N) - \gamma H, \\[2mm]
\frac{dA}{dt} &= (1 - \eta)\beta\frac{S}{N}(H + \phi A + \varrho N) - \gamma A, \\[2mm]
\frac{dR}{dt} &= \gamma(H + A) - \alpha R,
\end{aligned}
\tag{7}
$$

in which we have introduced also the import factor ϱ, which refers to the possibility of susceptible individuals becoming infected by an undetected infection chain which started outside the studied population [35, 36].

The stochastic version of the presented SHAR model is obtained analogously to the basic SIR model shown above [10], and the dynamics for the probabilities $p(\mathbf{x}, t)$ can once again be given as in Eq. (4).

In particular, for the basic SHAR model with import ϱ and eventual waning immunity α (which matters, e.g., when new variants affect natural immunity of the host), $\mathbf{x}$ is the state vector of densities $x_1 := S/N, x_2 := H/N, x_3 := A/N$ and $x_4 := R/N$, while the $n = 5$ transitions and corresponding shifting vectors are given by

$$
\begin{aligned}
w_1(\mathbf{x}) &= \eta\beta x_1(x_2 + \phi x_3 + \varrho) &&, \mathbf{r}_1 = (1, -1, 0, 0)^T \\
w_2(\mathbf{x}) &= (1 - \eta)\beta x_1(x_2 + \phi x_3 + \varrho) &&, \mathbf{r}_2 = (1, 0, -1, 0)^T \\
w_3(\mathbf{x}) &= \alpha(1 - x_1 - x_2 - x_3) &&, \mathbf{r}_3 = (-1, 0, 0, 1)^T \\
w_4(\mathbf{x}) &= \gamma x_2 &&, \mathbf{r}_4 = (0, 1, 0, -1)^T \\
w_5(\mathbf{x}) &= \gamma x_3 &&, \mathbf{r}_5 = (0, 0, 1, -1)^T,
\end{aligned}
\tag{8}
$$

(see, e.g., [29, 20, 49, 10, 47] for further details).

Figure 4 shows four snapshots in time (for $t = 10, 50, 60, 400$) of a single realization of the stochastic spatial SHAR model with import. Individuals are either susceptible (green), hospitalized (red), mild/asymptomatic infections (yellow) or re-

covered (blue). Assuming that the entire population (here $N = 10000$) is initially susceptible at $t = 0$, the import term introduces the infection, producing isolated outbreaks of different sizes. While some of these outbreaks involve only a few individuals and quickly die out, with all individuals recovering, others may involve many more active infections (severe and/or mild and asymptomatic), spreading widely and eventually collapsing with neighboring clusters, leading to much larger outbreaks. An exponential growth of cases is to be expected when the community transmission is super-critical. A detailed analysis of spatial dynamics using the SHAR framework is ongoing and preliminary results will be briefly discussed in the last section of this chapter. More details on the role of import in epidemic models can be found in [1, 47].
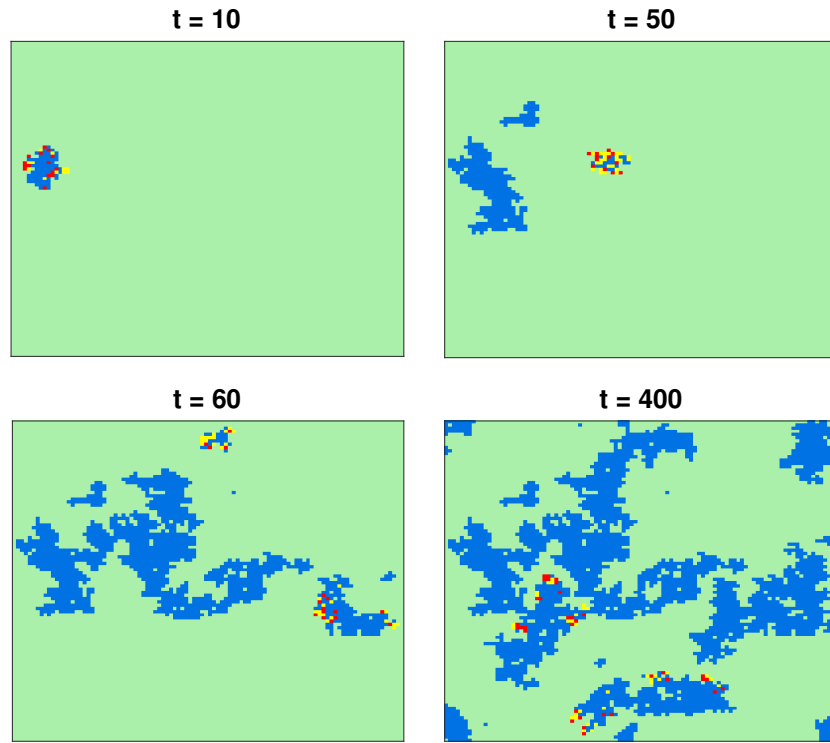

Fig. 4 Spatial configuration of a two-dimensional SHAR system with import at four different time points. The population of $N = 10000$ is divided into susceptible (green), hospitalized (red), asymptomatic (yellow), recovered (blue). Parameter values are: $\alpha = 0$, $\gamma = 1$, $\eta = 0.4$, $\beta = 0.85$, $\phi = 1.2$, and $\varrho = 10^{-9}$. Periodic boundary conditions are implemented.

2.2 The SHARUCD modeling framework

To describe the COVID-19 dynamics in the Basque Country, the basic SHAR model was extended by introducing the classes of Intensive Care Unit (ICU) admissions U and of deceased individuals D. Further, for comparison with the available cumulative empirical data, also the cumulative classes for hospitalized C_H, mild/asymptomatic infected C_A, ICU admitted C_U, and recovered C_R were included, counting all incoming cases in the dynamical compartments and neglecting the outflows. A detection ratio ξ for mild/asymptomatic cases was also considered, since a proportion of mild/asymptomatic cases are detected by contact tracing/screening testing, and hence the number of positive tested infections is larger than the notified hospitalized cases.

In this model, disease severity is decided upon infection with a proportion η developing severe infection prone to hospitalization (and $1 - \eta$ developing mild/asymptomatic infection). Undetected asymptomatic cases are assumed to transmit the disease more efficiently ($\phi > 1$) than severe cases. Hospitalized individuals can recover, with a recovery rate γ, die, with a mortality rate μ or go to an ICU facility, with an admission rate ν. Here, ICU admission is assumed to be a progression of disease severity after hospitalization.

The stochastic version of the basic SHARUCD model can be formulated through the master equation in the generic form of Eq. (4) with variables $x_1 := S/N$, $x_2 := H/N$, $x_3 := A/N$, $x_4 := R/N$, $x_5 := U/N$, $x_6 := C_H/N$, $x_7 := C_A/N$, $x_8 := C_U/N$ and $x_9 := D/N$ and $x_{10} := C_R/N$. The state vector $\mathbf{x} := (x_1, ..., x_{10})^T$ gives the dynamics for the probabilities $p(\mathbf{x}, t)$, with $n = 10$ different transitions. The transitions $w_j(\mathbf{x})$ and the corresponding shifting vectors $\mathbf{r}_j$ are given by

$$
\begin{aligned}
w_1(\mathbf{x}) &= \eta\beta x_1(x_2 + \phi x_3 + \varrho) & , \mathbf{r}_1 &= (1, -1, 0, 0, 0, -1, 0, 0, 0, 0)^T \\
w_2(\mathbf{x}) &= \xi(1 - \eta)\beta x_1(x_2 + \phi x_3 + \varrho) & , \mathbf{r}_2 &= (1, 0, -1, 0, 0, 0, -1, 0, 0, 0)^T \\
w_3(\mathbf{x}) &= (1 - \xi)(1 - \eta)\beta x_1(x_2 + \phi x_3 + \varrho) & , \mathbf{r}_3 &= (1, 0, -1, 0, 0, 0, 0, 0, 0, 0)^T \\
w_4(\mathbf{x}) &= \gamma x_2 & , \mathbf{r}_4 &= (0, 1, 0, -1, 0, 0, 0, 0, 0, -1)^T \\
w_5(\mathbf{x}) &= (1 - \xi)\gamma x_3 & , \mathbf{r}_5 &= (0, 0, 1, -1, 0, 0, 0, 0, 0, 0)^T \\
w_6(\mathbf{x}) &= \gamma x_5 & , \mathbf{r}_6 &= (0, 0, 0, -1, 1, 0, 0, 0, 0, -1)^T \\
w_7(\mathbf{x}) &= \nu x_2 & , \mathbf{r}_7 &= (0, 1, 0, 0, -1, 0, 0, -1, 0, 0)^T \\
w_8(\mathbf{x}) &= \mu x_2 & , \mathbf{r}_8 &= (0, 1, 0, 0, 0, 0, 0, 0, -1, 0)^T \\
w_9(\mathbf{x}) &= \mu x_5 & , \mathbf{r}_9 &= (0, 0, 0, 0, 1, 0, 0, 0, -1, 0)^T \\
w_{10}(\mathbf{x}) &= \xi\gamma x_3 & , \mathbf{r}_{10} &= (0, 0, 1, -1, 0, 0, 0, 0, 0, -1)^T \quad .
\end{aligned}
$$

$$(9)$$

The mean-field ODE system corresponding to the above $w_j(\mathbf{x})$ and $\mathbf{r}_j$ is given in [5, 53] and was used to evaluate the model performance, its accuracy, and to guide the modeling analysis.

The model was parameterized with empirical data provided by the Basque Health Department and the Basque Health Service (Osakidetza) for each disease-related variable. Parameters were estimated and fixed as the model was able to describe the disease incidence during the exponential phase of the outbreak, see Fig. 5.
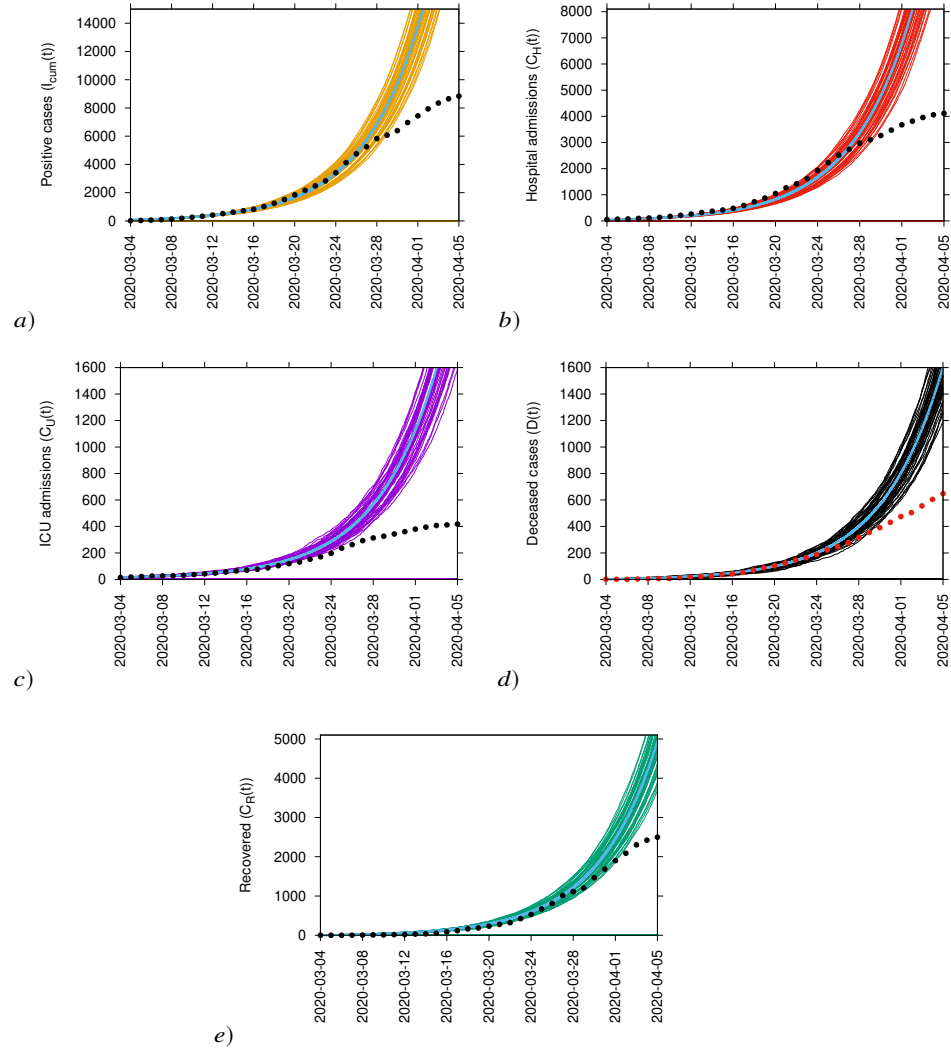
Fig. 5 From March 4 to April 4, 2020, ensemble of stochastic realizations of the baseline SHARUCD-model. The mean-field solution is shown in light blue. In a) cumulative detected positive cases $I_{cum}(t)$, in b) cumulative hospitalized cases $C_H(t)$, in c) cumulative ICU admissions $C_U(t)$, in d) cumulative deceased cases $D(t)$ and in e) cumulative recovered $C_R(t)$ (data on alive hospital discharges were used as a proxy for recovered individuals).

The stochastic realizations of the model are calculated via the Gillespie algorithm [30, 31]. To investigate the parameter uncertainties, we calculate numerically the likelihood functions for each parameter conditioned on the others and the data, evaluating distances between simulations and data from all five variables, $D(t)$, $I_{cum}(t)$, $C_H(t)$, $C_U(t)$ and $C_R(t)$, for the exponential phase of the epidemic. The detailed analysis for the parameter estimation and uncertainties via likelihood functions can be found in [5, 10, 53].

Partial lockdown was implemented in the Basque Country on March 16, 2020 with effects observed on March 27 (see Fig. 5) well before the full lockdown of March 31, 2020 [5]. With the initial parameters estimated and fixed on the exponential phase of the epidemic, the next step was to model the effect of the disease control measures to describe the gradual slowing down of the epidemic.

2.3 Modeling the implementation of control measures

The effect of the disease control measures was implemented by introducing for the infectivity parameter a smooth sigmoidal variation which was able to describe well the gradual slowing down of the epidemic, reaching negative growth rate at the end of March, 2020. Specifically, the infection rate β became a time dependent function $\beta(t)$ given by

$$\beta(t) = \beta_0 \sigma_- (x(t)) + \beta_1 \sigma_+ (x(t)), \qquad (10)$$

where $\sigma_-(x) = 1/(1 + e^x)$ and $\sigma_+(x) = 1/(1 + e^{-x})$ are downward and upward sigmoidal functions, respectively. The time dependent function $x(t)$ is defined by $x(t) = a(t - t_c)$ and gives the timing and speed of the implementation of control measures. Further refinements with respect to Eq. (10), considering other smooth sigmoidal variations, have been implemented over the course of the pandemic, as control measures were introduced or relaxed (e.g., from March 4 to July 10, 2020, the profile of $\beta(t)$ is given in Fig. 6 with a smooth reduction of the transmission rate for the lockdown implementation and a later smooth increase corresponding to the gradual lockdown lifting). Low seasonality was also assumed to play a role, helping to keep transmission at low levels. For more details, please visit our SHARUCD Dashboard page [53].

Figure 7 shows an ensemble of stochastic realizations considering the effective control measures given by Eq. (10), up to mid April, 2020. A good agreement was obtained for hospitalization, deceased cases and recovered, with data lying in the median range of the 200 stochastic realizations. Notice that the deviation observed for the detected positive class I_{cum} is expected, due to the increased testing capacity started in March 22. The system was not adjusted to include the non-hospitalized cases. Moreover, the erratic behavior of the ICU admission cases remained to be investigated.

Using the data at hand, the momentary growth rates were calculated, see Figures 8 a) and b), and compared with the momentary reproduction ratio, see Fig. 8 c), confirming a negative growth of infection at the end of March, 2020 [12]. Two types
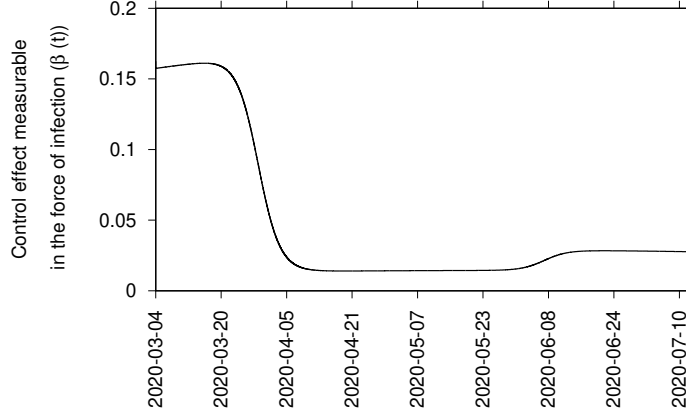
Fig. 6 Smooth variations in the infection rate $\beta = \beta(t)$ reproducing the effect of control measures, considering small seasonality. Parameters values are shown in Table 1. For the lockdown effect, $a = 0.38\ d^{-1}$ and $t_c = 25$ days after the initial time t_0 (corresponding here to March 4, 2020). For the lockdown lifting, $a_2 = 0.16\ d^{-1}$ and $t_{c_2} = 112$ days after t_0.

of behavior were observed: positive cases, hospitalization and, surprisingly, also the ICU admissions with the same sigmoidal decrease, shown in Fig. 8 a), whereas the deceased and recovered were delayed for 8 and 10 days, respectively, shown in Fig. 8 b).

This finding lead us to refine the baseline SHARUCD framework by changing the ICU admission rate ν into a ratio, with COVID-19 infection causing from asymptomatic up to very severe cases prone to hospitalization and to ICU admission.

2.4 The refined SHARUCD model

If previously it was assumed that hospitalized patients could either recover with recovery rate γ, be admitted to an ICU facility with rate ν, or die with disease-induced death rate μ, in light of the analysis of the momentary growth rates presented above, the baseline SHARUCD model was refined by considering ICU admissions to be a consequence of infection leading to severe disease, with a patient being immediately admitted to an ICU facility upon infection with ratio ν, analogously to the ratio η for hospitalizations. Note that although most of the hospitalizations were recovering or dying, some of those cases would eventually evolve into ICU cases and that was accounted for in the model as well.

The refined model is given by changes in the transition rates of the stochastic version, see [12], such that now the transition to ICU admission is synchronized with the transition to hospitalization and to the cumulative positive cases. Specifically, the transitions
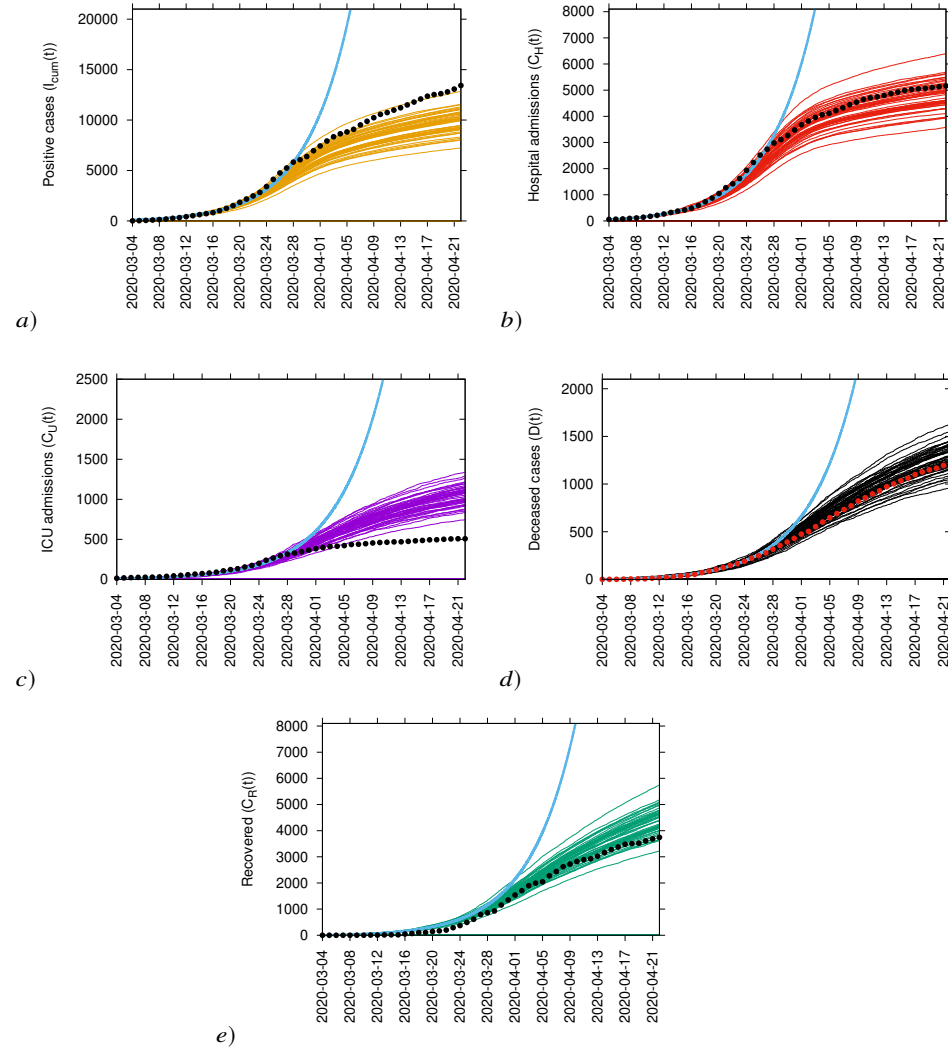
Fig. 7 From March 4 to April 21, 2020, ensemble of stochastic realizations of the baseline SHARUCD-model. The mean-field solution without control is shown in light blue. In a) cumulative detected positive cases $I_{cum}(t)$, in b) cumulative hospitalized cases $C_H(t)$, in c) cumulative ICU admissions $C_U(t)$, in d) cumulative deceases cases $D(t)$ and in e) cumulative recovered $C_R(t)$ (hospital discharges alive data were used as a proxy for recovered individuals).
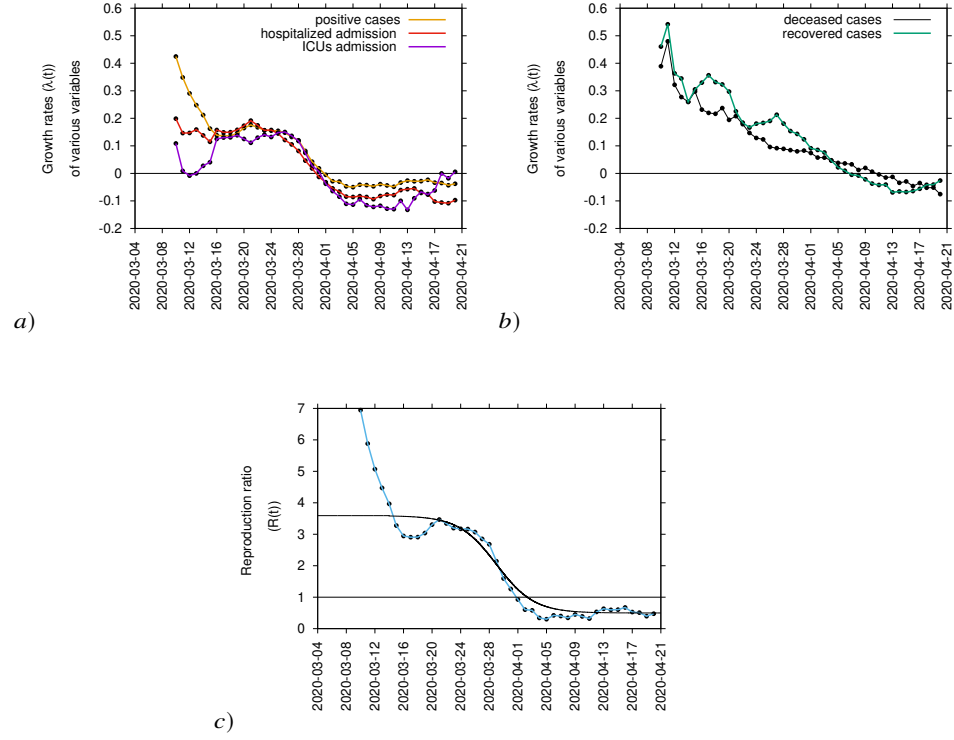
a)

b)

c)

Fig. 8 From March 4 to April 21, 2020, the momentary growth rates for various variables shows two types of behavior. In a) detected positive cases in yellow, hospitalized cases in red, and ICU admissions in purple, cross the threshold on April 1, 2020. In b) recovered cases in green and deceased cases in black, cross the threshold with a delay of 8 and 10 days, respectively. The momentary reproduction ratio is shown in c).

$$w_1(\mathbf{x}) = \eta\beta x_1(x_2 + \phi x_3 + \varrho) \ , \ \mathbf{r}_1 = (1, -1, 0, 0, 0, -1, 0, 0, 0, 0)^T$$
$$w_7(\mathbf{x}) = \nu x_2 \qquad\qquad\qquad , \ \mathbf{r}_7 = (0, 1, 0, 0, -1, 0, 0, -1, 0, 0)^T \qquad (11)$$

are changed into

$$w_1(\mathbf{x}) = \eta(1-\nu)\beta x_1(x_2 + \phi x_3 + \varrho) \ , \ \mathbf{r}_1 = (1, -1, 0, 0, 0, -1, 0, 0, 0, 0)^T$$
$$w_7(\mathbf{x}) = \eta\nu\beta x_1(x_2 + \phi x_3 + \varrho) \qquad , \ \mathbf{r}_7 = (1, 0, 0, 0, -1, -1, 0, -1, 0, 0)^T , \qquad (12)$$

with the parameter ν being adjusted from the ICU admission rate in units of d^{-1} into an ICU admission ratio $\nu \in [0, 1]$. The deterministic version of the model is hence given by

$$\frac{d}{dt}S = -\beta\frac{S}{N}(H + \phi A + \varrho N)$$

$$\frac{d}{dt}H = \eta(1 - \nu)\beta\frac{S}{N}(H + \phi A + \varrho N) - (\gamma + \mu)H$$

$$\frac{d}{dt}A = (1 - \eta)\beta\frac{S}{N}(H + \phi A + \varrho N) - \gamma A$$

$$\frac{d}{dt}R = \gamma(H + U + A) \tag{13}$$

$$\frac{d}{dt}U = \nu\eta\beta\frac{S}{N}(H + \phi A + \varrho N) - (\gamma + \mu)U$$

$$\frac{d}{dt}C_H = \eta\beta\frac{S}{N}(H + \phi A + \varrho N)$$

$$\frac{d}{dt}C_A = \xi \cdot (1 - \eta)\beta\frac{S}{N}(H + \phi A + \varrho N)$$

$$\frac{d}{dt}C_R = \gamma(H + U + \xi A)$$

$$\frac{d}{dt}C_U = \nu\eta\beta\frac{S}{N}(H + \phi A + \varrho N)$$

$$\frac{d}{dt}D = \mu(H + U)$$

which is now able to describe the dynamics of the ICU admissions as well as the ones for hospitalized and deceased cases [5], see Fig. 9.

Notice that the mean-field approximation of the stochastic system is given by the deterministic version in Eq. (13) (see [50]). For a complete analysis of the model, the reader is referred to [10]. Simulations of the stochastic SHARUCD model can be performed via the Gillespie algorithm [30, 31]. Figure 9 shows an ensemble of stochastic realizations for the COVID-19 epidemic in the Basque Country, from March 4, to June 16, 2020. The basic parameter values used for simulation of the model are shown in Table 1.

2.4.1 Further refinements: detection rate and import

At the onset of the pandemic, data on COVID-19 infections were reflecting only severe cases requiring hospitalization, while the knowledge of asymptomatic and mild positive cases became available at a later stage, when testing capacity increased. This information heavily relies on local testing capacity and strategy, and is therefore highly variable in both time and space. To adjust to the observed deviation on the detected positive class I_{cum}, see Fig. 9 a), due to the increased testing capacity over time, see Fig 10 a), the refined model considers a time dependent detection ratio ξ assumed to be small in the introductory phase of the epidemic but later increased to a much higher level.

As testing capacity increased, the system was not able to describe quantitatively well the data for the recovered class R, since the hospital discharges data used as
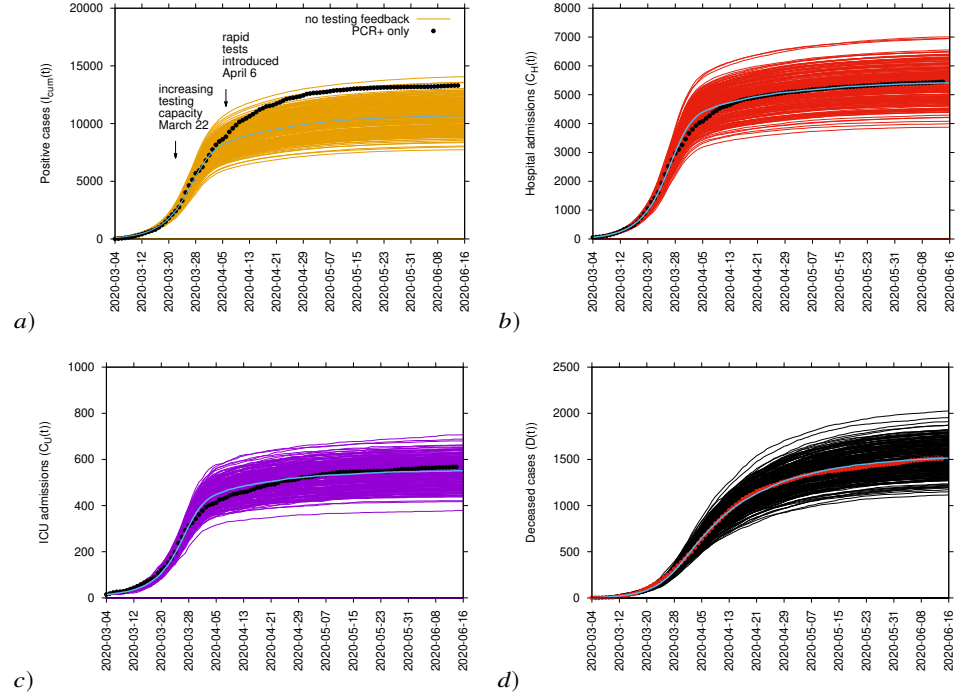
Fig. 9 From March 4 to June 16, 2020, ensemble of stochastic realizations of the refined SHARUCD-model. The mean-field solution is shown in light blue. In a) cumulative detected positive cases $I_{cum}(t)$, in b) cumulative hospitalized cases $C_H(t)$, in c) cumulative ICU admissions $C_U(t)$, and in d) cumulative deceased cases $D(t)$.

proxy for recovered individuals did not include the recovered individuals which were eventually tested positive but did not need hospitalization.

The model was also refined to describe isolated outbreaks after lockdown lifting, describing well the dynamics for positive detected cases, hospitalizations, ICU admission and deceased cases from March 4 to December 31, 2020, shown in Fig. 1.

We assume that an imported case is most likely a mobile asymptomatic infected individual, either a foreigner visiting the region or a local returning to the country without being detected by the current testing strategy, similarly to what one expects when country lockdowns are completely lifted and mobility is possible again. The so-called imported cases would be needed to describe the introductory phase of the epidemic, but we did not have any information on that at the start of exponential growth of the COVID-19 epidemic. The import factor becomes important again, after the full lockdown is lifted, allowing human mobility and asymptomatic disease transmission [1, 47]. For the present study, we assume ϱ to be much smaller than the other additive terms of the force of infection, given the strong observational insecurities on the data collected at the beginning of the outbreak.
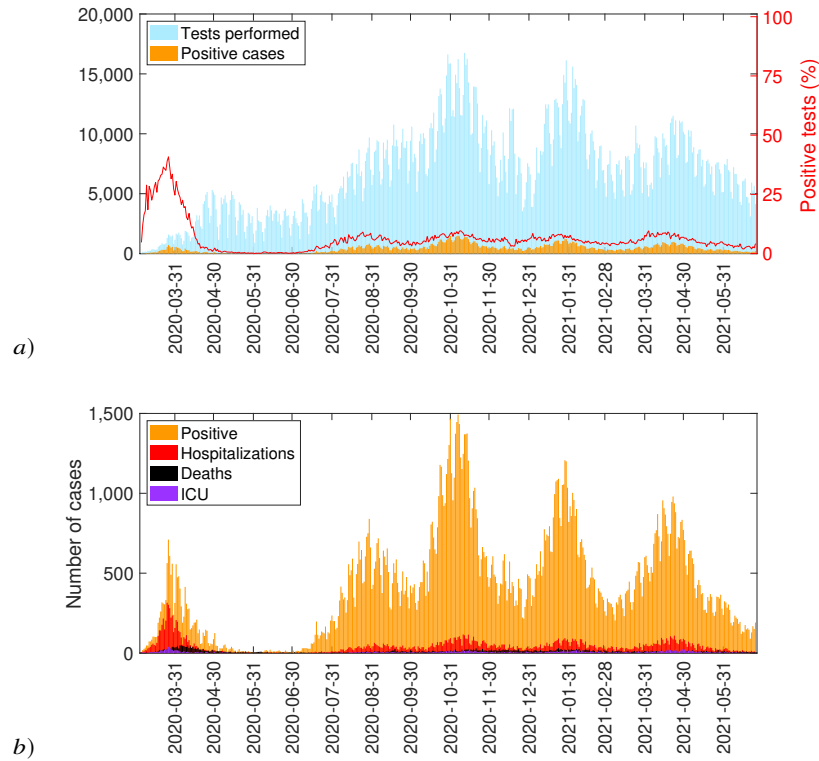
Fig. 10 From March 4 to June 24, 2021, in a) COVID-19 tests performed in the Basque Country (light blue), positive PCR cases (yellow) and positivity rate (red line). In b) COVID-19 detected cases in the Basque Country: Positive PCR cases are shown in yellow, hospitalizations in red, ICU admissions in purple, and deceased cases in black.

Table 1 summarizes the starting parameter set used to describe the COVID-19 epidemic in the Basque Country from March 4, 2020. As it was previously mentioned in this chapter, model refinements were implemented during the course of the pandemic, with β, ξ and ϱ becoming time dependent parameters as non-pharmaceutical intervention actions were introduced and lockdown measures were implemented and relaxed over time. Therefore, it is important to mention that small adjustments on the presented parameter set were needed and with these small modifications we were able to match well data until December 31, 2020, as shown in Fig. 1. For further details, readers are referred to the SHARUCD Dashboard and references therein.

As a continuation of the BMTF efforts, the vaccination trial data for the vaccines which have been licensed for emergency use in Europe is evaluated. Results are implemented into the simple SHAR modeling framework and its extensions to get the

Table 1 SHARUCD model parameters

Model basic parameter	Description	Reference value
β	infection rate	$3.25 \cdot \gamma$
γ	recovery rate	$0.05 d^{-1}$
η	proportion of hospitalization	0.075
ν	ICU admission ratio	0.09
ϕ	ratio of mild/asymptomatic infections contributing to force of infection	1.65
ξ	detection rate	$[0.01 - 0.95]$
μ	disease-induced death rate	$0.02 d^{-1}$
ρ	import	0.0006

qualitative overview of the impact of COVID-19 vaccination strategy in the Basque Country [51]. These results will be briefly described in the discussion section of this chapter and, for more details, readers are referred to [51].

3 KTAP modeling framework

The model presented in the previous section considers disease transmission at the population level. However, describing disease progression at the microscopic scale is also important and informative for the evaluation of pharmaceutical interventions for example, such as antiviral/antibiotics administration and vaccination. For instance, to investigate the infection process in a population of target cells, considering the immunological response of the host, the so-called *within-host* modeling framework is needed. Some recommended readings on this topic are [38, 39], and references therein, which introduce essential concepts on cell biology and immunology.

For respiratory diseases that cause damage to the lungs, like COVID-19, models should describe the dynamics of the viral load which might lead to different asymptotic trends between full recovery and death by overload and even material corruption of the lung. A description of the dynamics of the lung in order to detect those areas which are more susceptible to stretch overload in the pulmonary parenchyma is provided in [22]. Some useful recent contributions in this line are [33], which presents an interactive COVID-19 tissue simulator of viral dynamics of SARS-CoV-2 in a layer of epithelium, and [56] where a community-driven tissue simulator is developed.

Modeling ought to be developed within a multiscale approach. On the one hand, the dynamics of contagion must be treated at the macro-scale level of individuals and populations, while on the other, the evaluation of the state of each individual (healthy, infectious, etc.) depending on the infection dynamics of the body cells as a result of the immunological response against the pathogen, should be analyzed at the micro-scale level.

Both scales constantly interact and that is probably one of the most valuable virtues of the model presented in [17] and further refined in [4, 19], since the contagion at the macro-scale depends on the viral load of each individual, which in turn depends on the dynamics at the micro-scale. The model is based on the kinetic theory of active particles [18], and hereinafter will be referred to as the KTAP model.

The general framework supporting the KTAP modeling approach is defined by a selection of key features discussed in detail in the technical report [23]:

1. Individuals are viewed as *active particles* (a-particles) which are carriers of an internal state, called *activity*. In particular, the micro-state of every individual is described by a variable w corresponding to the level of activation of the immune defence. In addition, infected individuals are also characterized by a variable u representing the level of progression of the infection (ranging from mild to severe).

2. Contagion depends on the level of the infection as well as on an infection rate. The latter, as in the SHARUCD model, may be a time dependent parameter that takes into account the implementation of specific health policies, like social distancing, lockdowns, etc.

3. The progression of the infection within each individual depends on the interaction between the pathogen replication and the immune response.

3.1 Modeling contagion, progression, and recovery

Let us consider a population of N individuals homogeneously distributed in space. Each individual can belong, at time t, to one of the following compartments or functional subsystems (FS): susceptible (S-FS), infected (I-FS), recovered (R-FS) or deceased (D-FS). The S-FS is assumed to have only an outflow (into the I-FS), while R-FS and D-FS only have an inflow (from I-FS), i.e., we assume that recovered individuals get a long-lasting immunity and remain in that compartment.

The microscopic state of each individual entity is characterized by a variable $w \in [0, 1]$ describing the level of activation of the immune defence. It is worth stressing that in the original formulation of the model the value of w for a given individual does not change over time. In order to simplify the identification of subgroups (or clusters of a-particles as in [21]) according to the individuals' immune response level (e.g., reflecting age or presence of comorbidities), the variable w is typically discretized and assumed to take values in the set

$$I_w = \{w_1 = 0, \dots, w_k = \frac{k-1}{n-1}, \dots, w_n = 1\}.$$

Within the I-FS class, individuals are also described by a variable $u \in [0, 1]$, which corresponds to the within-host progression of the pathogen invasion. Considering discrete values also for u in the set

$$I_u = \{u_1 = 0, \ldots, u_j = \frac{j-1}{m-1}, \ldots, u_m = 1\},$$

we have that $u_1 = 0$ describes the absence of the infection, while $u_j > 0$ indicates the presence of the disease with a variation of infection level. Increasing values of u towards 1 describe more aggressive states that may end up in the death of the host when reaching $u_m = 1$.

The number of immune levels n can be chosen by considering possible ways to disaggregate the population into age classes or morbidity groups, depending on the case under study (see e.g., [13, 9]). On the other hand, m shall take into account the number of stages of a given disease after the initial entry of the pathogen into the host. In order to have all three compartments I, D, and R in the modeling framework, it is assumed that $m \geq 3$.

The dynamics is such that susceptible individuals, characterized by their micro-state w_k, may become infected after an interaction with an infected a-particle. Within the I-FS, an a-particle is characterized by the pair (u_j, w_k), with $2 \leq j \leq m - 1$. A competitive interaction between the pathogen and the immune system then starts and the transition into R-FS or D-FS depends on the result of this dynamics: namely, if the state u_1 (resp. u_m) is reached, the individual undergoes a transition into the recovered (resp. deceased) compartment. This is illustrated in Fig. 11.
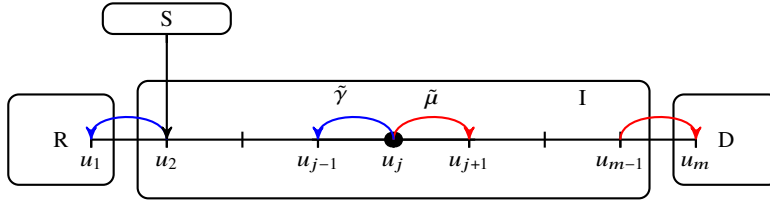

Fig. 11 Illustration of the transitions: susceptible individuals can get infected with an infection rate $\tilde{\beta}$, entering to the infected compartment (wide box in the middle) with state u_2. Then, competitive interactions between the pathogen that replicates with rate $\tilde{\mu}$ towards more aggressive infection states and the immune system, which acts with rate $\tilde{\gamma}$, with resulting transition into the R or D compartment.

The representation of the system is given by the following distribution functions:

- $f_S^k(t)$ is the probability to find, at time t, a susceptible individual with micro-state w_k. The susceptible population at time t, $f_S(t)$, is simply computed as the sum $\sum_{k=1}^n f_S^k(t)$.
- $f_I^{j,k}(t)$ is the probability to find, at time t, an infected individual with micro-state (u_j, w_k). The prevalence of infection, at time t, is given by $f_I(t) = \sum_{k=1}^n \sum_{j=2}^{m-1} f_I^{j,k}$.
- $f_R^k(t)$ is the probability to find, at time t, a recovered individual with micro-state w_k. The cumulative recovered population $f_R(t)$ is simply computed as the sum $\sum_{k=1}^n f_R^k(t)$.

- $f_D^k(t)$ is the probability to find, at time t, a deceased individual with micro-state w_k. As for the recovered, the cumulative deceased population $f_D(t)$ is given by $\sum_{k=1}^{n} f_D^k(t)$.

Notice that $f_S(t) + f_I(t) + f_R(t) + f_D(t) = 1$ for all t and that the actual number of individuals belonging to each FS can be computed multiplying the distribution function by the total population N.

The dynamics of the system is described by using tools of the mathematical structures of the kinetic theory of active particles, see e.g., Chapter 5 in [16]. The system of equations representing the evolution of the distribution functions, whose derivation can be followed in details in [17], is given by:

$$
\begin{cases}
\dfrac{d}{dt} f_S^k(t) = -\tilde{\beta} \sum_{s=1}^{n} \sum_{j=2}^{m-1} u_j\, f_S^k(t)\, f_I^{j,s}(t), \\[2ex]
\dfrac{d}{dt} f_I^{j,k}(t) = \tilde{\beta}\, \delta_{2j} \left(\sum_{s=1}^{n} \sum_{p=2}^{m-1} u_p\, f_S^k(t)\, f_I^{p,s}(t) \right) + \tilde{\mu}\, u_{j-1}\, f_I^{j-1,k}(t) \\[1ex]
\qquad\qquad + \tilde{\gamma}\, w_k\, f_I^{j+1,k}(t) - \tilde{\mu}\, u_j\, f_I^{j,k}(t) - \tilde{\gamma}\, w_k\, f_I^{j,k}(t), \\[2ex]
\dfrac{d}{dt} f_R^k(t) = \tilde{\gamma} \sum_{k=1}^{n} w_k\, f_I^{2,k}(t), \\[2ex]
\dfrac{d}{dt} f_D^k(t) = \tilde{\mu}\, u_{m-1} \sum_{k=1}^{n} f_I^{m-1,k}(t),
\end{cases}
\tag{14}
$$

where for the first equation we have $k = 1, \ldots, n$, while for the second one $j = 2, \ldots, m-1$ and $k = 1, \ldots, n$. The first equation in (14) describes the infection of susceptible individuals due to interactions with infected ones. The second equation in (14) describes the dynamics within the infected population. The factor δ_{2j} denotes a Kronecker delta, meaning that the entry state upon infection is u_2. From that point, a competitive interaction between the pathogen and the immune system starts. Finally, the third and fourth equations give the inflows into recovered and deceased classes, respectively, as a result of the aforementioned competitive interactions. Regarding model parameters, $\tilde{\beta}$ is the infection rate, $\tilde{\mu}$ is the pathogen progression rate and $\tilde{\gamma}$ is the immune action rate towards recovery.

An extension of the system in Eq. (14) to networks can be found in [4].

3.2 Application of the KTAP model to selected case studies

The KTAP model introduced above has been applied to a variety of exploratory experiments aiming to understand the role of population heterogeneity in the propagation of the disease with an insight in non-pharmaceutical interventions (NPI) [17]

and vaccination [19]. In this section, we present some selected case studies focusing on the intensity and timing of NPI and on the heterogeneity of the population, represented by the micro-states w_k.

In the following, let us consider a population of $N = 2.2$ million individuals (a-particles in this context). At time $t = 0$ almost all of them belong to the S-FS, with 100 a-particles in the I-FS, while R-FS and D-FS are empty. We consider $n = 5$ classes, in agreement with a possible choice among demographers and epidemiologists to disaggregate a population into age groups, but other possibilities can also be considered [13]. Although n and m need not be the same, here we also set $m = 5$.

Effect of lockdown measures and restrictions lifting

Let us first study the effect of lockdown measures, in order to understand how the amplitude and timing of the action influences the overall dynamics. The lockdown implementation is modeled by a reduction of the infection rate $\tilde{\beta}$ during a given time interval.

Figure 12 shows the dynamics of cumulative infected cases up to a given T_{max} for three different scenarios. In all three cases, the pathogen replication rate and the immune action rate are kept constant and equal to $\tilde{\mu} = 0.008$ and $\tilde{\gamma} = 0.03$, respectively.

In Fig. 12 a) the infection rate $\tilde{\beta}$ is initially equal to 0.6. At locking time $T_l = 25$, the effect of a lockdown is modeled by reducing the transmission rate $\tilde{\beta}$ to 0.06 until a reopening time $T_o = 50$ at which $\tilde{\beta}$ is increased to β_o. The curves corresponding to three different values of β_o are shown in the plot, up to $T_{max} = 100$.

Fig. 12 b) shows a similar situation in which a lockdown is implemented, reducing the transmission rate $\tilde{\beta}$ from 0.6 to 0.06 at different locking times $T_l = 25, 30, 40$, giving an insight on the the importance of intervention measures timing.

In Fig. 12 c) we consider three different opening times $T_o = 50, 70, 90$ at which the infection rate $\tilde{\beta}$ is increased back from 0.06 to 0.6. Notice that the three curves increase towards large values approaching N, showing that a late reopening without control leads to a delayed explosion of infections. Here, $T_{max} = 200$ for visualization purposes.

Effect of heterogeneity

Let us now study the effect of heterogeneity in the population by considering different distributions of immunity, which is a proxy for age and presence of other comorbidities.

The left panels of Fig. 13 show three possible immunity distributions: a centered symmetric distribution, describing a population with an average immunity level, a distribution which is skewed to the right, describing a population having a stronger immune system (e.g., a younger population), and one that is skewed to the left, describing a population having a weaker immune system (e.g., a vulnerable population
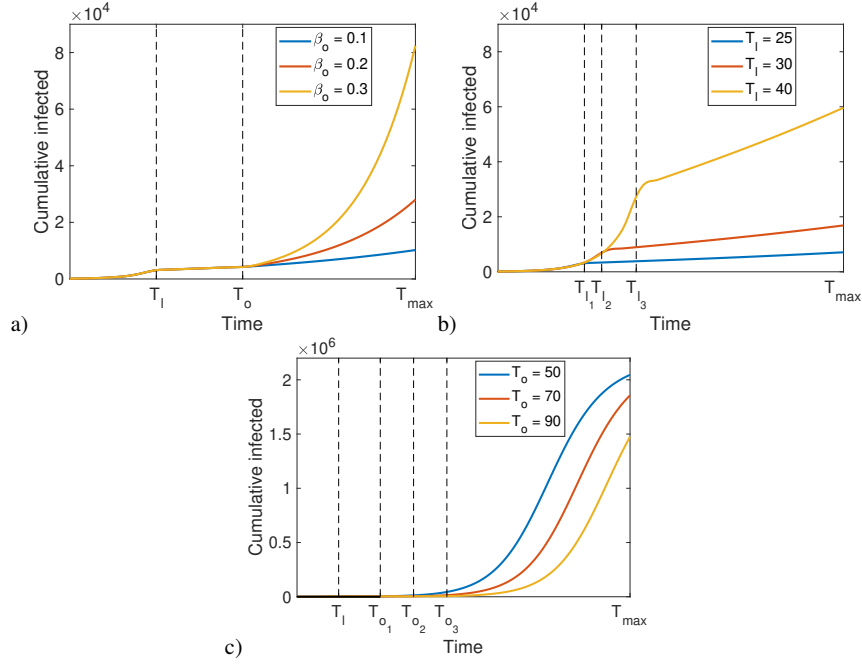
Fig. 12 Influence of lockdown measures and restrictions lifting. In a) the transmission rate $\tilde{\beta}$ is reduced from 0.6 to 0.06 at locking time $T_l = 25$ and then increased again, at opening time $T_o = 50$, to different values β_o. In b) the lockdown is implemented at three different locking times, with reduction of $\tilde{\beta}$ from 0.6 to 0.06. In c) $\tilde{\beta}$ is increased back to 0.6 at three different opening times T_o. The other parameter values are $n = m = 5$, $\tilde{\gamma} = 0.03$ and $\tilde{\mu} = 0.008$.

composed by elderly individuals). In [4] these distributions are used to describe, respectively, populations in households, schools and nursing homes.

On the right panel of Figure 13 we can see the dynamics for cumulative infected (left axis), recovered and deceased cases (right axis) for the initial exponential phase for the three distributions of w_k shown on the left. The set of parameters is the same as above (with $\tilde{\beta} = 0.6$ unchanged during the considered time span), while the initial conditions reflect the distribution of w_k for each case. Notice that the immunity distribution actually influences the number of infected, recovered and deceased cases, since larger (resp. lower) values of w_k lead, eventually, to a faster recovery (resp. decease).

Finally, we perform an exercise to study the correlation between population heterogeneity and infection. Let us define the mean immune level by $\sum_{k=1}^{n} w_k f^k$, where f^k is the probability to find an a-particle with state w_k. In our case, $f^k = f_S^k + \sum_{j=1}^{m} f_I^{j,k} + f_R^k + f_D^k$ does not change with time due to the assumption that particles keep their micro-state w_k.

The scatter plot in Fig. 14 shows a strong positive (resp. negative) correlation between the mean immune level and the recovered (resp. deceased) for 500 realizations
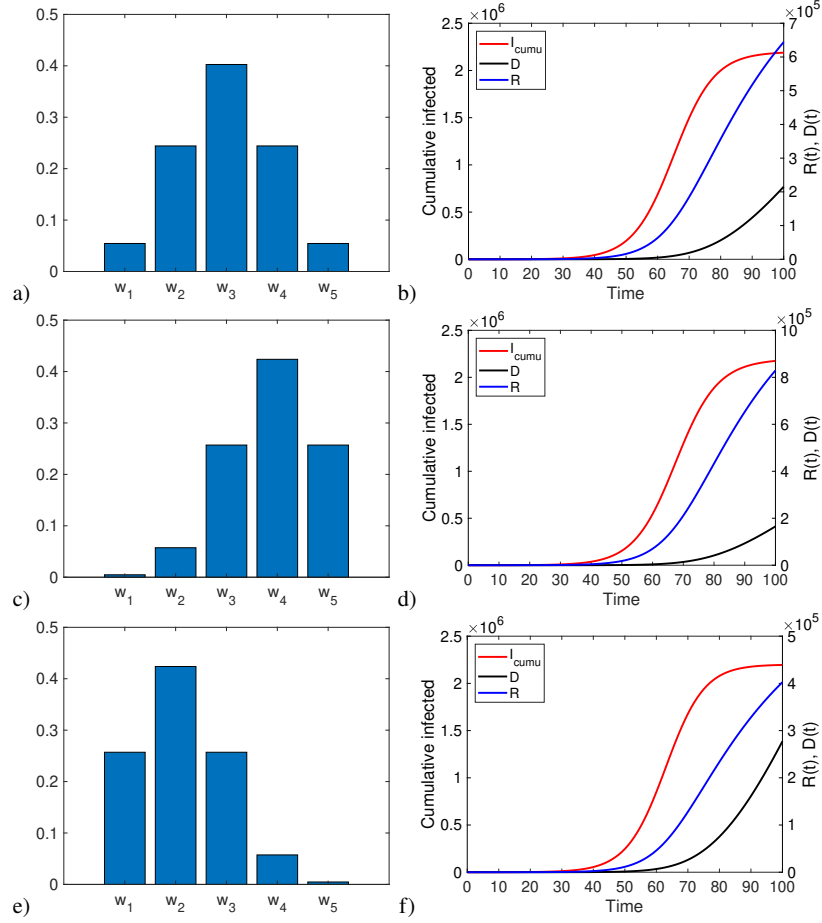
Fig. 13 The left panel shows the frequency distribution of immunity levels w_k in three cases: a) centered, c) skewed right, e) skewed left. On the right panel we show the cumulative infected (left axis), recovered and deceased cases (right axis) for the corresponding distributions on the left. No interventions are assumed in this case and the infection rate is fixed at $\tilde{\beta} = 0.6$.

of the following experiment: the distribution of w_k is randomly chosen to define the initial conditions and the mean immune level is computed, then the KTAP model is run with the parameters $\tilde{\beta} = 0.6, \tilde{\gamma} = 0.03, \tilde{\mu} = 0.008$ up to $T_{max} = 100$. A marker represents the recovered and deceased cases at T_{max} for that particular immune level. This result emphasizes the role of heterogeneity and will be further discussed in the next section in the context of vaccination strategies.
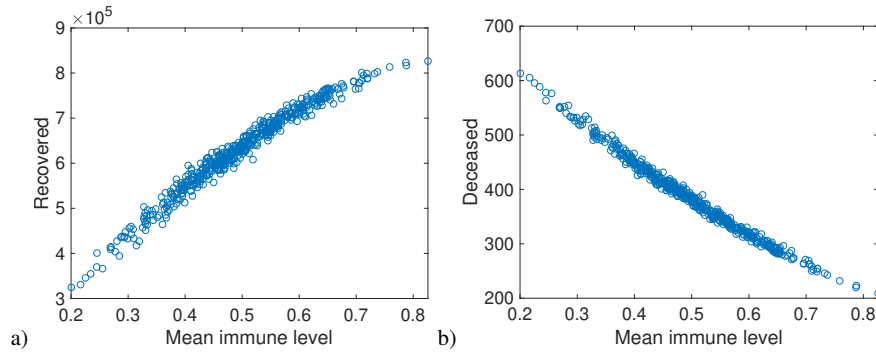
Fig. 14 Recovered and deceased cases at final time for different mean immune levels. The immunity distribution is chosen randomly for each of the 500 realizations of the experiment.

4 Discussion

In the previous sections we have presented two different approaches to model the spread of an epidemic. The SHARUCD modeling framework introduced in Section 2 was developed within the Basque Modeling Task Force. As an extension of the basic SIR-type epidemiological models, the SHARUCD model stratifies the class of infected individuals into severe/hospitalized cases H and mild/asymptomatic A, and includes further classes for intensive care unit admissions U and deceased D. The stochastic SHARUCD model can be regarded as a predictive model which successfully describes the COVID-19 epidemic in the Basque Country in terms of disease spreading and control, as shown in Fig. 1. The model is currently used to monitor COVID-19 transmission in the Basque Country (the complete model is described in details in [5, 53]) and was able to provide accurate projections on the regional health system's necessities during the first wave of the pandemic and beyond. As explained in Section 2, the SHARUCD model was refined to analyze isolated outbreaks [1, 47], including now import to asymptomatic infection, after lifting of lockdowns, and increased detection of asymptomatic due to increasing testing capacity.

Investigation on critical fluctuations around the epidemiological threshold has shown that the lockdown measures implemented in the autumn 2020 were able to drive the growth of COVID-19 cases to the so called sub-critical regime of community transmission, leading to a low notification of severe cases, up to the end of October 2020, and kept in stationarity even when the overall transmission rate increased by an enhanced mobility. The same behavior was also observed in different European regions [1, 47].

This study is a baseline for the understanding of the impact of the current vaccination programs around the globe giving insights on the role of community transmission and mobility regarding the reduction of severe disease. The system can be also evaluated under different vaccine efficacies and coverage, while population immunity is acquired by natural infection and vaccination, until finally reaching the

so-called herd immunity threshold. The SHARUCD framework is under refinement to include the uneven vaccination roll-out strategy currently in place worldwide with preliminary results described in [51].

We use the epidemiological SHAR model framework to evaluate the effects of vaccination in different epidemiological scenarios of coverage and efficacy. Two vaccination models (one protecting against severe disease and the other protecting against infection as well as severe disease) are compared to evaluate the reduction of overall infections and hospitalizations. Differences in vaccine efficacy and coverage must be also considered for a more accurate evaluation of vaccine performance. Our results show that in an intermediate scenario of low to medium vaccination coverage and limited vaccine efficacy, vaccine performance will be influenced by the transmission level of mild and asymptomatic cases [51]. These results and concepts are of use to study also the epidemiological situation of vaccine waning immunity and immune escape by new variants.

On the other hand, the KTAP approach presented in Section 3 has so far been applied with exploratory purposes to model an infectious disease where a pathogenic agent spreads among a population of target cells, trying to evade the immune response. In this sense, the model is quite simple not even considering the nature of target cells (e.g., mainly gut and lung cells in the case of SARS-CoV-2 infection [15, 46]). However, this modeling approach can be adapted to explore different scenarios considering multi-scale features and heterogeneity of the population by stratifying it, e.g., according to age or comorbidities. For example, in [4] the population is distributed over a network where each node has a different social structure type: school, household, working place, and nursing home. Interactions can be modeled according to this stratification using, for example, mixing matrices [21, 37].

It is worth stressing that, if no heterogeneity is considered in the KTAP model (meaning $n = 1$) and only three levels of infection severity are considered (i.e., $m = 3$), we get, as a particular case, the SIR-type model configuration shown in Fig. 15. In this case, we can relate the dependent variables from both models as: $f_S(t) \approx x_1(t)$, $f_I(t) \approx x_2(t) + x_3(t) + x_5(t)$, $f_R(t) \approx x_4(t)$ and $f_D(t) \approx x_9(t)$ (see Eq. (9)).
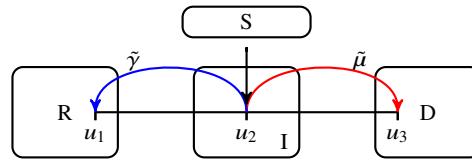

Fig. 15 Schematic representation of the simplified KTAP model with $n = 1$ and $m = 3$.

A subsequent step is to relate the viral replication in the KTAP approach with the different compartments in the SHARUCD model, schematized in Fig. 16, and to properly model transitions not only between adjacent states but also to distant ones (for instance, a patient who has been immediately admitted to ICU facility

upon infection). This perspective gives also an insight into a possible further stratification in the SHARUCD model, considering, e.g., age groups or accounting for subpopulations with comorbodities.
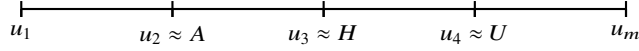

Fig. 16 Different severity levels of the disease.

Finally, as vaccination against COVID-19 proceeds, both models introduced in this present chapter are under refinement to investigate the impact of population immunity by vaccination.

The KTAP approach has also been applied to conduct an exploratory analysis on the impact of vaccination targeting a given population. In [4] the effect of vaccination was modeled by "moving" some individuals with low w values to the highest level w_n. When the number of vaccinated particles increases, a strong reduction in terms of infected and deceased cases is observed, with a large negative correlation between the variables. This result confirms the relationship shown in Fig. 14 and the importance of immunization. In order to take into account the dynamics of the roll-out of vaccines, ongoing research assumes the micro-states w_k to be time dependent.

Adding a spatial component to the models considered above is another way to introduce an additional scale into the modeling framework. Spatial dynamics is required in certain settings, e.g., when wanting to study differences in disease transmission dynamics depending on geographical location or when looking at the combined impact on transmission of different local/regional public health policies.

In Section 2 of this chapter, we have illustrated the effect of an import term in the stochastic and spatially-dependent SHAR model. While in the non-spatial context determining the critical threshold of community transmission can be done analytically, in the spatially-dependent case this is no longer possible and one has to measure such threshold numerically instead. In general, a deviation from the corresponding mean-field approximation is to be expected since spatial correlations alter the results.

This type of analysis for the models presented in this chapter is ongoing and will be discussed in detail in our forthcoming publications.

Acknowledgements

References

1. Aguiar, M., Bidaurrazaga Van-Dierdonck, J., Mar, J., Cusimano, N., Knopoff, D., Anam, V., Stollenwek, N.: Critical fluctuations in epidemic models explain COVID-19 post-lockdown dynamics. Sci. Rep. **11**, 13839 (2021)
2. Aguiar, M., Bidaurrazaga Van-Dierdonck, J., Stollenwerk, N.: Reproduction ratio and growth rates: measures for an unfolding pandemic. PLoS ONE **15**, e0236620 (2020)
3. Aguiar, M., Coelho, G.E., Mateus, L., Rocha, R., Pessanha, J.E.M., Mateus, L., Stollenwerk, N.: Dengue transmission during the 2014 FIFA World Cup in Brazil. Lancet Infect. Dis. **10**, 765–766 (2015)
4. Aguiar, M., Dosi, G., Knopoff, D., Virgillito, M.E.: A multiscale network-based model of contagion dynamics: heterogeneity, spatial distancing and vaccination. Math. Mod. Meth. Appl. Sci., to appear (2021)
5. Aguiar, M., Millán Ortuondo, E., Bidaurrazaga Van-Dierdonck, J., Mar, J., Stollenwek, N.: Modelling COVID 19 in the Basque Country from introduction to control measure response. Sci. Rep. **10**, 17306 (2020)
6. Aguiar, M., Paul, R., Sakuntabhai, A., Stollenwerk, N.: Are we modeling the correct data set? Minimizing false predictions for dengue fever in Thailand. Epidemiol. Infect. **142**, 2447–59 (2014)
7. Aguiar, M., Stollenwerk, N.: Dengvaxia efficacy dependency on serostatus: a closer look at more recent data. Clin. Infect. Dis. **66(4)**, 641–642 (2018)
8. Aguiar, M., Stollenwerk, N.: Dengvaxia: age as surrogate for serostatus. Lancet Infect. Dis. **18(3)**, 245 (2018)
9. Aguiar, M., Stollenwerk, N.: Condition-specific mortality risk can explain differences in COVID-19 case fatality ratios around the globe, Public Health **188**, 18–20 (2020)
10. Aguiar, M., Stollenwerk, N.: SHAR and effective SIR models: from dengue fever toy models to a COVID-19 fully parametrized SHARUCD framework. Commun. Biomath. Sci. **3(1)**, 60–89 (2020)
11. Aguiar, M., Stollenwerk, N.: The Impact of Serotype Cross-Protection on Vaccine Trials: DENVax as a Case Study. Vaccines **8**, 674 (12 pages) (2020)
12. Aguiar, M., Stollenwerk, N., Halstead, S.B.: Modeling the impact of the newly licensed dengue vaccine in endemic countries. PLoS Neglect. Trop. D. **10(12)**, e0005179 (2016)
13. Ahmad, O.B *et al.* Age standardization of rates: A new WHO standard, GPE Discussion Paper Series, World Health Organization, **31**, (2001).
14. Baden, L.R., El Sahly, H.M., Essink, B. *et al.*: Efficacy and Safety of the mRNA-1273 SARS-CoV-2 Vaccine, New Engl. J. Med. **384**, 403–416 (2021)
15. Baraniuk, C.: Receptors for SARS-CoV-2 Present in Wide Variety of Human Cells (2020) Available via TheScientist.
https://www.the-scientist.com/news-opinion/receptors-for-sars-cov-2-present-in-wide-variety-of-human-cells-67496. Cited 13 Apr 2021
16. Bellomo, N., Bellouquid, A., Gibelli, L., Outada, N.: A Quest Towards a Mathematical Theory of Living Systems. Birkhäuser, New York (2017).

17. Bellomo, N., Bingham, R., Chaplain, M., Dosi, G., Forni, G., Knopoff, D., Lowengrub, J., Twarock, R., Virgillito, M.: A multiscale model of virus pandemic: Heterogeneous interactive entities in a globally connected world. Math. Mod. Meth. Appl. Sci. **30**, 4591–1691 (2020)

18. Bellomo, N., Burini, D., Dosi, G., Gibelli, L., Knopoff, D., Outada, N., Terna, P. and Virgillito, M.E.: What is life? A perspective of the mathematical kinetic theory of active particles. Math. Models Methods Appl. Sci., (2021) doi: 10.1142/S0218202521500408.

19. Bellomo, N., Burini, D., Outada, N.: Multiscale models of COVID-19 with mutations and variants. Netw. Heterog. Media, to appear (2021)

20. Billings, L., Mier-y-Teran-Romero, L., Lindley, B., Schwartz, I: Intervention-based stochastic disease eradication, arXiv:1303.5614v1 (2013)

21. Blyuss, K., Kyrychko, Y.: Effects of latency and age structure on the dynamics and containment of COVID-19. J. Theor. Biol. **513**, 110587 (2021)

22. Carloni, A., Poletti, V., Fermo, L., Bellomo, N., Chilosi, M.: Heterogeneous distribution of mechanical stress in human lung: A mathematical approach to evaluate abnormal remodeling. J. Theor. Biol. **332**, 136–140 (2013)

23. Cecconi, M., Forni, G., Mantovani, A.: COVID-19: An executive report April 2020 update. Accademia Nazionale dei Lincei, Commissione Salute (2020)

24. Cucinotta D., Vanelli M.: WHO Declares COVID-19 a Pandemic. Acta Biomed. **91**, 157–160 (2020)

25. Dagan, N., Barda, N., Kepten, E. *et al.*: BNT162b2 mRNA Covid-19 Vaccine in a Nationwide Mass Vaccination Setting, New Engl. J. Med. **384**, 1412–1423 (2021)

26. Davies, N.G., Klepac, P., Liu, Y., Prem, K., Jit, M.: Age-dependent effects in the transmission and control of COVID-19 epidemics. Nat. Med. **26**, 1205–1211 (2020)

27. Davies, N.G., Kucharski, A.J., Eggo, R.M., Gimma, A., Edmunds, W.J.: Effects of non-pharmaceutical interventions on COVID-19 cases, deaths, and demand for hospital services in the UK: a modelling study. Lancet Publ. Health **5**, e375–e385 (2020)

28. European Medicines Agency. COVID-19 vaccines: authorised.
https://www.ema.europa.eu/en/human-regulatory/overview/public-health-threats/coronavirus-disease-covid-19/treatments-vaccines/vaccines-covid-19/covid-19-vaccines-authorised Cited 12 May 2021

29. Gang, H.: Stationary solution of master equations in the large-system-size limit. Phys. Rev. A **36**, 5782–5790 (1987)

30. Gillespie, D.T.: A general method for numerically simulating the stochastic time evolution of coupled chemical reactions. J. Comput. Phys. **22**, 403–434 (1976)

31. Gillespie, D.T.: Monte Carlo simulation of random walks with residence time dependent transition probability rates. J. Comput. Phys. **28**, 395–407 (1978)

32. Goldstein, E., Lipsitch, M., Cevik, M.: On the effect of age on the transmission of SARS-CoV-2 in households, schools and the community. J. Infect. Dis. **223**, 362–369 (2020)

33. Heiland, R., Wang, Y., Macklin, P.: Prototype 2-D multicellular simulation of COVID19. In: https://nanohub.org/resources/32987/ (2021)

34. Johns Hopkins Coronavirus Resource Center. (n.d.). COVID-19. Johns Hopkins University & Medicine. In https://coronavirus.jhu.edu/us-map. Cited 15 Apr, 2020

35. Mateus, L., Ghaffari, P., Skwara, U., Rocha, F., Aguiar, M., Masoero, D., Stollenwerk, N.: Semiclassical approximations of stochastic epidemiological processes towards parameter estimation using as prime example the SIS system with import. Ecol. Complex. **27**, 63–73 (2016)

36. Mateus, L., Masoero, D., Rocha, F., Aguiar, M., Skwara, U., Ghaffari, P., Zambrini, J.C., Stollenwerk, N.: Epidemiological models in semiclassical approximation: an analytically solvable model as a test case. Math. Method. Appl. Sci. **39(16)**, 4914–4922 (2016)

37. McBryde, E., Trauer, J., Adekunle, A., Ragonnet, R., Meehan, M.: Stepping out of lockdown should start with school re-openings while maintaining distancing measures. Insights from mixing matrices and mathematical models, (2020) doi: 10.1101/2020.05.12.20099036 (2020)

38. Musiani, P., Forni, G.: Basic Immunology 2020 In: Issuu (2020) Available via ISSUU. https://issuu.com/guidoforni5/docs/2019o

39. Nowak, M.A., May, R.: Virus Dynamics: Mathematical Principles of Immunology and Virology. Oxford University Press, Oxford, (2001)
40. Pinto, A., Aguiar, M., Martins, J., Stollenwerk, N.: Dynamics of Epidemiological Models. Acta Biotheor. **58(4)**, 381–389 (2010)
41. Pollack, F., Thomas, S., Kitchin, N., *et al.*: Safety and efficacy of the BTN162b2 mRNA Covid-19 Vaccine. New Engl. J. Med. **383(27)**, 2603–2615 (2021) 10.1056/NEJMoa2034577.
42. Prem, K., Cook, A.R., Jit, M.: Projecting social contact matrices in 152 countries using contact surveys and demographic data. PLoS Comput. Biol. **13**, 1–21 (2017)
43. Roser, M., Ritchie, H., Ortiz-Ospina, E., Hasell, J.: Coronavirus Pandemic (COVID-19) (2021) Available at OurWorldInData.org.
    https://ourworldindata.org/coronavirus
44. Rozhnova, G., van Dorp, C.H., Bruijning-Verhagen, P. *et al.*: Model-based evaluation of school- and non-school-related measures to control the COVID-19 pandemic. Nat. Commun. **12**, 1614 (2021)
45. Sadoff, J., Gray, G., Vandebosch, A. *et al.*: Safety and Efficacy of Single-Dose Ad26.COV2.S Vaccine against Covid-19, New Engl. J. Med., (2021) doi: 10.1056/NEJMoa2101544
46. Shang, J., Wan, Y., Luo, C., Ye, G., Geng, Q., Auerbach, A., Li, F.: Cell entry mechanisms of SARS-CoV-2. P. Natl. Acad. Sci. USA **117(21)**, 11727–11734, (2020)
47. Stollenwerk, N., Bidaurrazaga Van-Dierdonck, J., Mar, J., Eguiguren Arrizabalaga, I., Cusimano, N., Knopoff, D., Anam, V., Aguiar, M.: The interplay between subcritical fluctuations and import: understanding COVID-19 epidemiological dynamics, medRxiv (2021). doi: 10.1101/2020.12.25.20248840
48. Stollenwerk, N., Briggs, K.M.: Master equation solution of a plant disease model. Phys. Lett. A **274**, 84–91 (2000)
49. Stollenwerk, N, Fuentes Sommer, P., Kooi, B., Mateus, L., Ghaffari, P., Aguiar, M.: Hopf and torus bifurcations, torus destruction and chaos in population biology. Ecol. Complex. **30**, 91–99 (2017)
50. Stollenwerk, N., Jansen, V.: Population Biology and Criticality: From Critical Birth–Death Processes to Self-Organized Criticality in Mutation Pathogen Systems. World Scientific, London (2011)
51. Stollenwerk, N., Mar, J., Bidaurrazaga Van-Dierdonck, J., Ibarrondo, O., Estadilla, C., Aguiar, M.: Modeling COVID-19 vaccine efficacy and coverage towards herd-immunity in the Basque Country, Spain. medRxiv (2021). doi: 10.1101/2021.07.12.21260390
52. Stollenwerk, N.,van Noort, S., Martins, J., Aguiar, M., Hilker, F., Pinto, A., Gomes, G.: A spatially stochastic epidemic model with partial immunization shows in mean field approximation the reinfection threshold. J. Biol. Dynam. **4(6)**, 634–649 (2010)
53. The Epidemiological SHARUCD Model Dashboard.
    https://wp.bcamath.org/news/en/epidemiological-sharucd-model/#introduction. Cited 23 Jul 2021
54. van Kampen, N.G.: Stochastic Processes in Physics and Chemistry. North-Holland, Amsterdam (1992)
55. Voysey, M., Clemens, S., Mahdi, S., *et al.*: Safety and efficacy of the ChAdOx nCov-19 vaccine (AZD1222) against SARS-CoV-2: an interim analysis of four randomized controlled trials in Brazil, South Africa and the UK. Lancet **397**, 10269 99–111 (2021)
56. Wang, Y. *et al.*: Rapid community-driven development of a SARS-CoV-2 tissue simulator. bioRxiv (2020). doi: 2020.04.02.019075
57. WHO Coronavirus (COVID-19) Dashboard.
    https://covid19.who.int/ Cited 12 May 2021
58. World Health Organization. Naming the Coronavirus Disease (COVID-19) and the Virus that Causes it.
    https://www.who.int/emergencies/diseases/novel-coronavirus-2019/technical-guidance/naming-the-coronavirus-disease-%28covid-2019%29-and-the-virus-that-causes-it
    Cited 31 Jan 2021

59. World Health Organization. WHO announces COVID-19 outbreak a pandemic.
    https://www.euro.who.int/en/health-topics/health-emergencies/coronavirus-covid-
    19/news/news/2020/3/who-announces-covid-19-outbreak-a-pandemic Cited 31 Jan 2021
60. World Health Organization. Coronavirus disease (COVID-19) Weekly Epidemiological
    Update and Weekly Operational Update https://www.who.int/emergencies/diseases/novel-
    coronavirus-2019/situation-reports Cited 23 Jul 2021
61. COVID-19 to Plunge Global Economy into Worst Recession since World War II. Available
    via The World Bank.
    https://www.worldbank.org/en/news/press-release/2020/06/08/covid-19-to-plunge-global-
    economy-into-worst-recession-since-world-war-ii Cited 12 May 2021